Electronic supplementary information for

Lattice Strain Controlled Ni@NiCu Efficient Anode Catalysts for Direct Borohydride Fuel Cell

Bihao Hu[a], Yuxin Xie[a], Ying Yang[a], Jiazhi Meng[a], Jinliang Cai[a], Changguo Chen[a], Danmei Yu[a], Xiaoyuan Zhou[b]**

[a] School of Chemistry and Chemical Engineering, Chongqing University, Chongqing, 401331, P.R. China

[b] College of Physics, Chongqing University, Chongqing, 401331, P.R. China

Corresponding Authors

***Danmei Yu's** e-mail: yudanmei-1@163.com.

***Xiaoyuan Zhou's** e-mail: xiaoyuan2013@cqu.edu.cn.

Notes: The authors declare no competing financial interest.

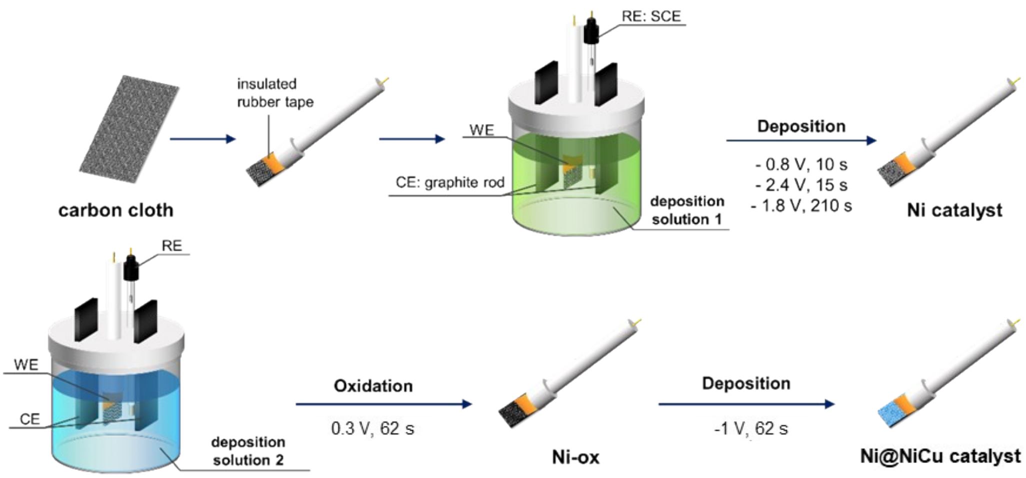

Fig. S1 Schematic diagram of the preparation catalysts.

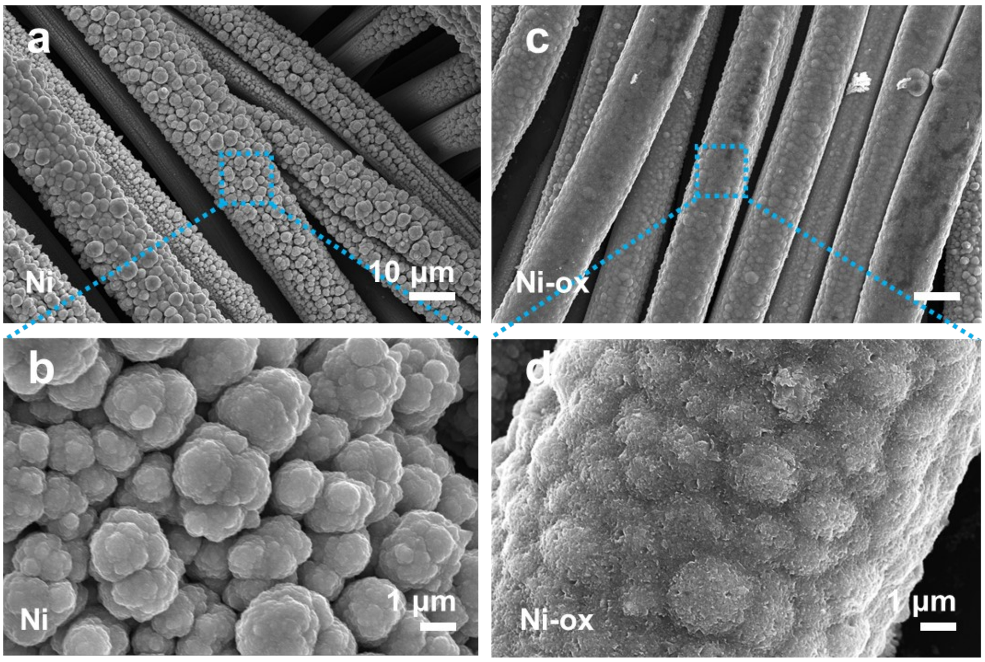

Fig. S2 (a) The SEM images and (b) the enlarged view of the Ni catalyst; (c) the SEM images and (d) the enlarge view of the Ni catalyst after oxidation (Ni-ox).

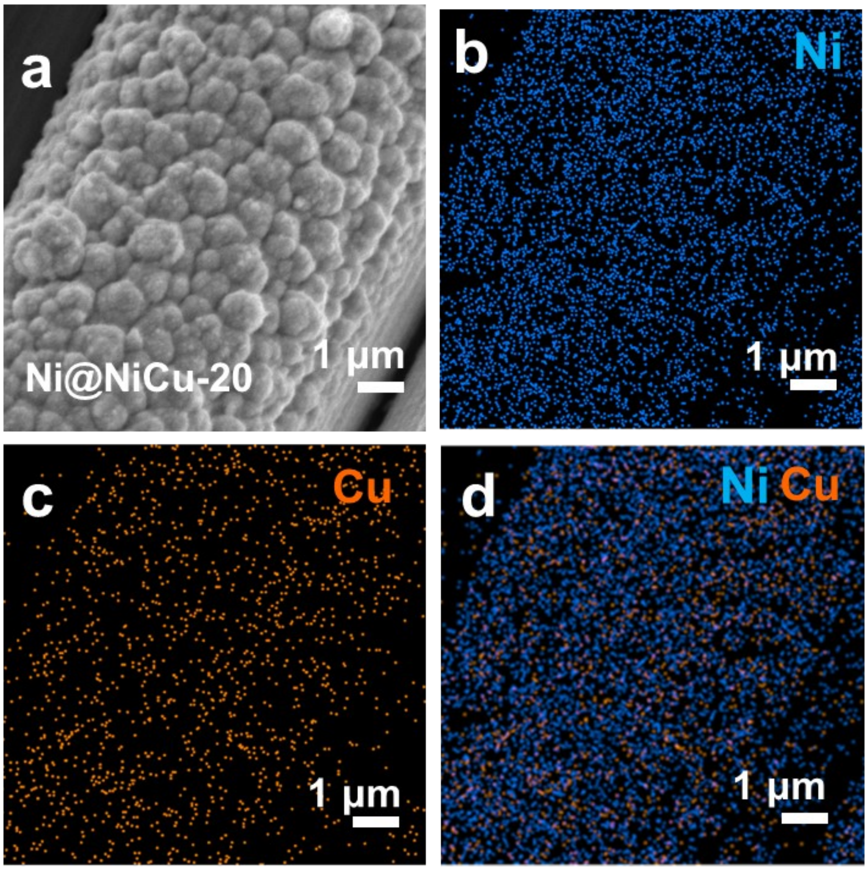

Fig. S3 (a) The SEM image of Ni@NiCu and (b-d) corresponding EDS element distribution mappings.

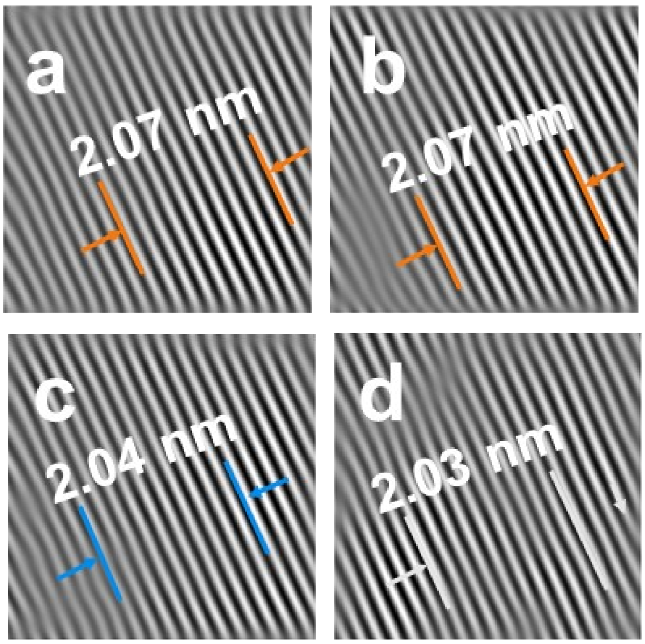

Fig. S4 (a-d) Processed lattice fringe images of boxes 1, 2, 3 and 4 in Fig. 2(a), respectively.

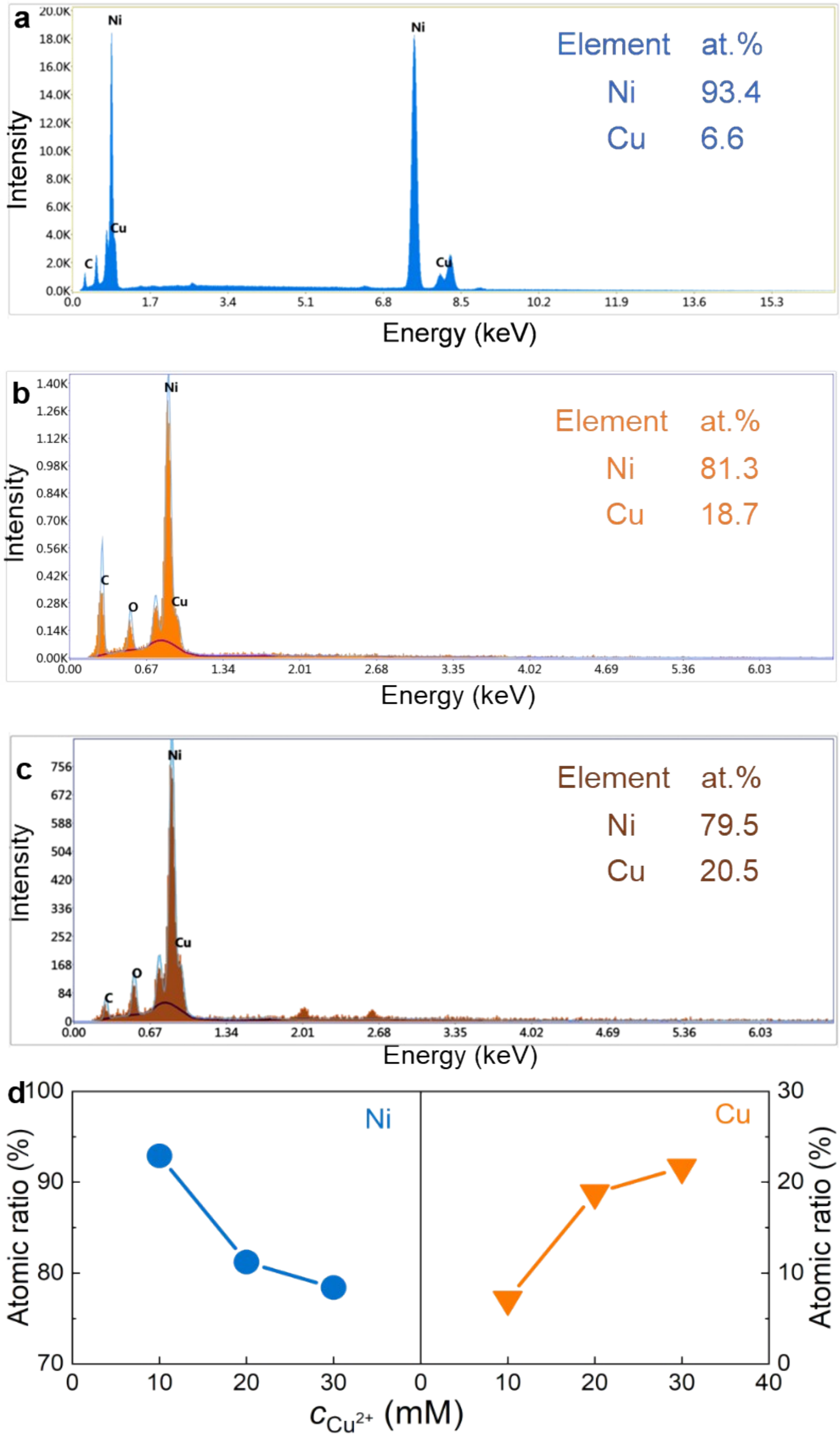

Fig. S5 SEM-EDS patterns of (a) Ni@Ni-10, (b)Ni@Ni-20, (c)Ni@Ni-30. (d) The correlation curves between the Cu^{2+} concentration in deposition solution and the contents of Ni and Cu in the Ni@NiCu-x catalysts.

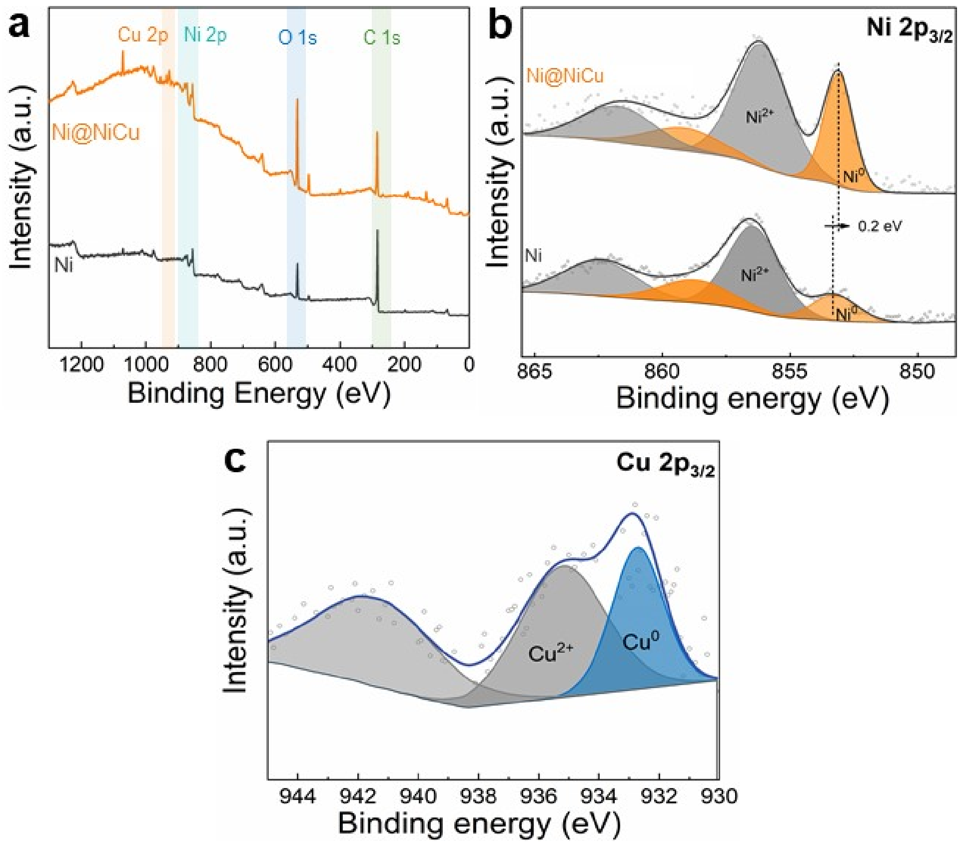

Fig. S6 (a) XPS surveys, (b) spectrums of Ni $2p_{3/2}$, and (c) Cu $2p_{3/2}$ of Ni and Ni@NiCu catalysts.

The effect of tensile lattice stain on the electronic structure of Ni surface is evaluated by X-ray photoelectron spectroscopy (XPS), shown in Fig. S6. The peaks near 853 eV and 858.5 eV are corresponded to the metallic Ni (Ni^0) and its satellite peaks,[1] while the peaks near 856.5 eV and 862 eV are attributed to Ni^{2+} and its satellite peaks.[2] Moreover, the Cu^0 and Cu^{2+} peaks in Ni@NiCu are located around 932.6 eV and 935.1 eV, respectively.

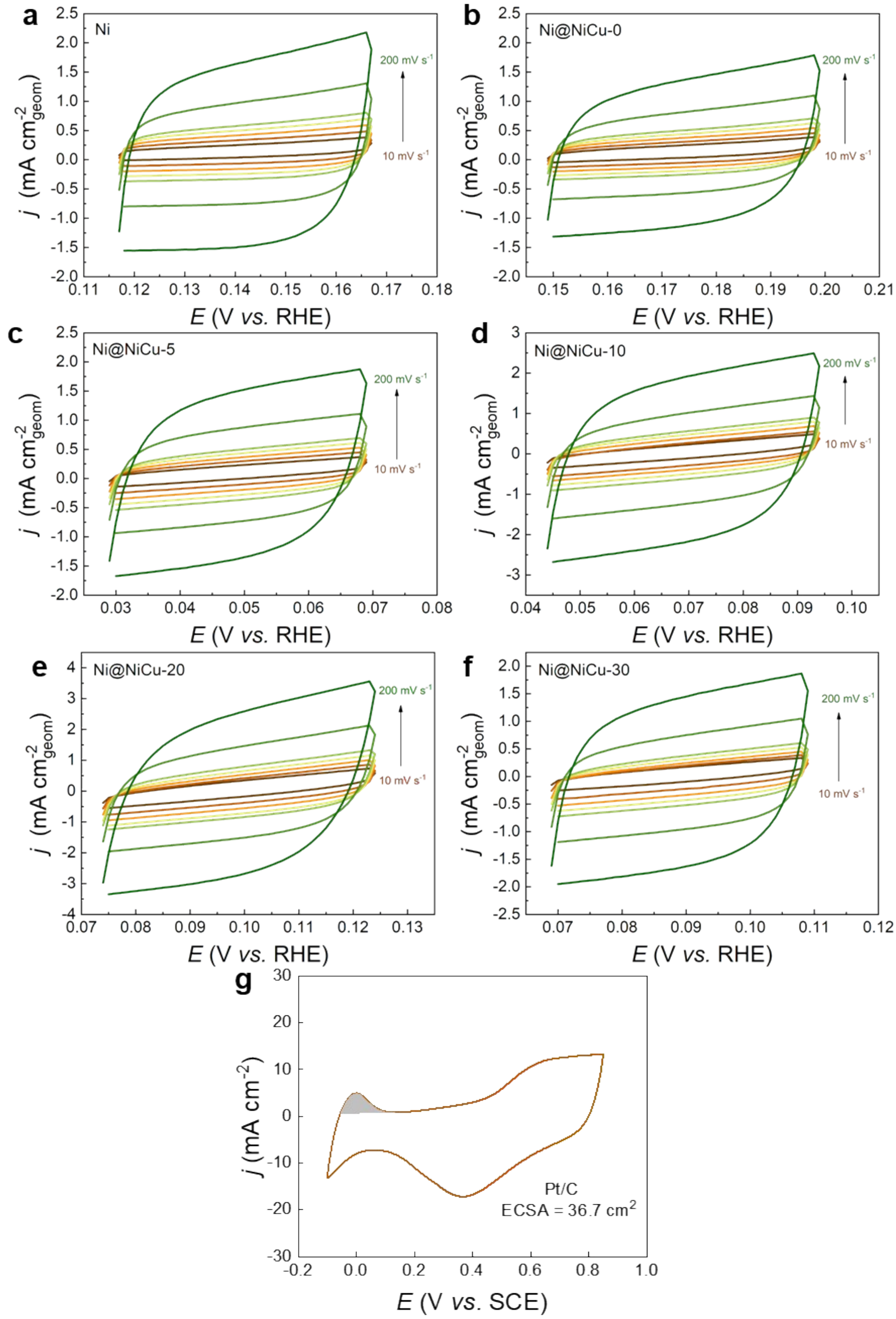

Fig. S7 CV curves on (a) Ni, (b) Ni@NiCu-0, (c) Ni@NiCu-5, (d) Ni@NiCu-10, (e) Ni@NiCu-20, (f) Ni@NiCu-30 catalysts in 1 mol L^{-1} NaOH solution at various scan rates, and (g) CV curve on Pt/C in 0.1 M $HClO_4$ at a scan rate of 50 mV s^{-1}. ECSA of Pt/C was calculated from a hydrogen adsorption peak from CV based on the equation: ECSA = Q_H/ (210 μC cm^{-2}), where Q_H is the charge of hydrogen electro-adsorption calculated from the shaded area.

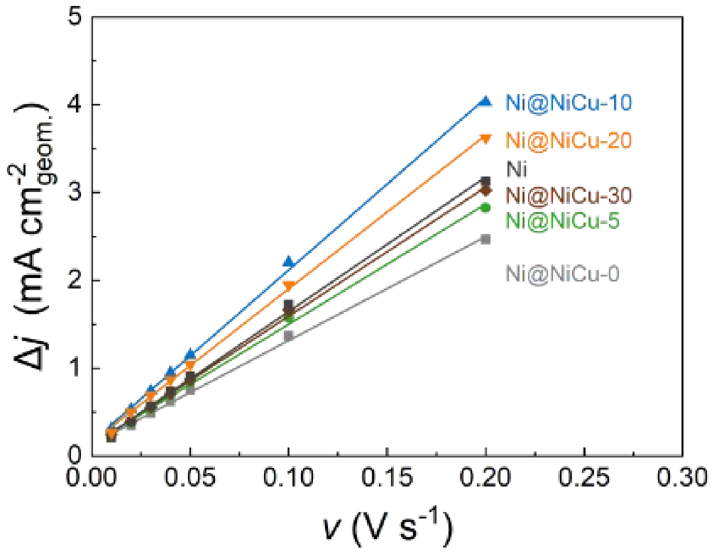

Fig. S8 The $v \sim \Delta j$ relationship curves on different catalysts.

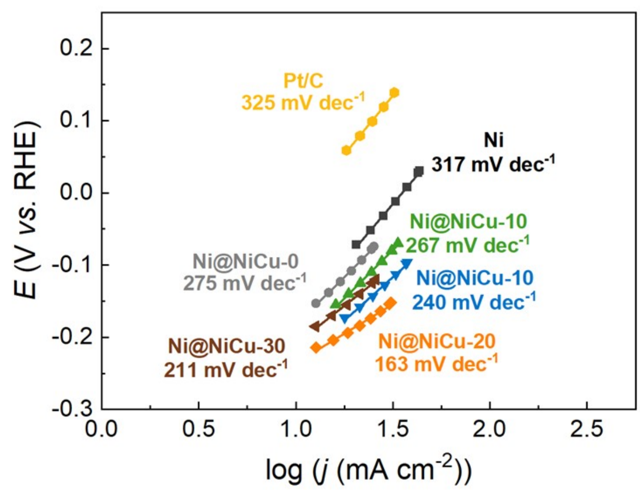

Fig. S9 The Tafel curves of BOR on Ni@NiCu-x, Ni, and commercial Pt/C catalysts in mixed a solution of 0.15 M $NaBH_4$ and 2 M NaOH at 25 ℃.

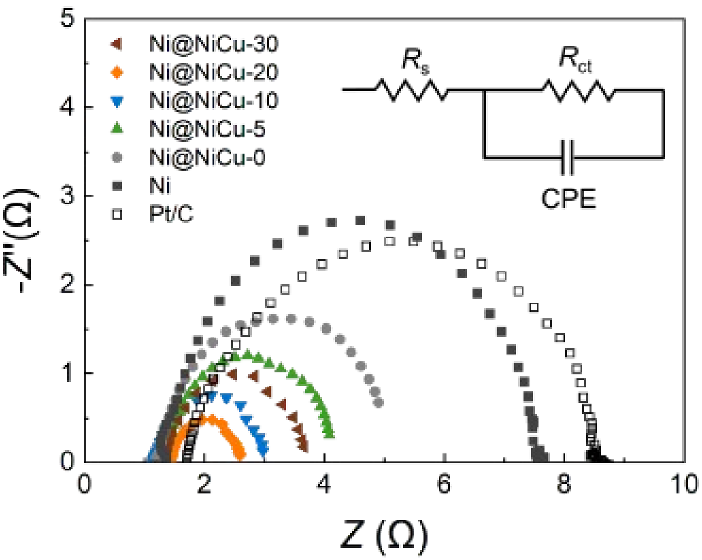

Fig. S10 The EIS of BOR on Ni@NiCu-x, Ni, and commercial Pt/C catalysts in 0.15 M $NaBH_4$ and 2 M NaOH mixed solution at 25 °C. The inset is the equivalent circuit.

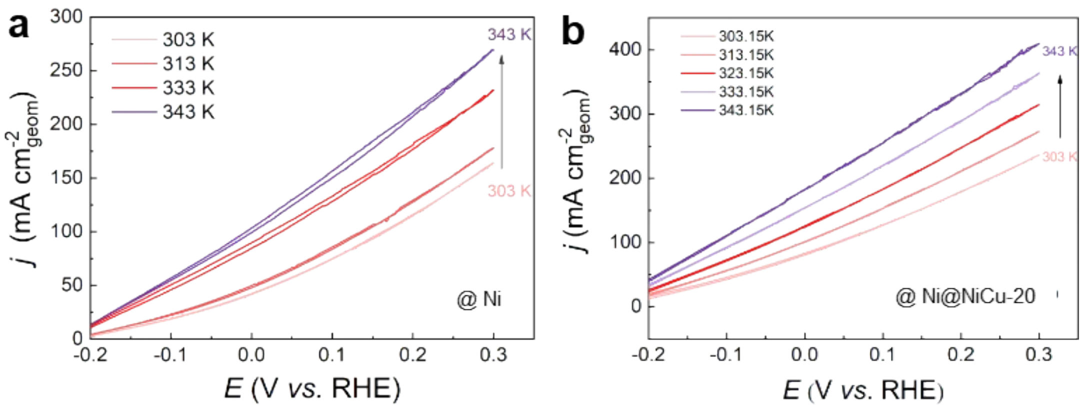

Fig. S11 The CV curves of BOR on (d) Ni and (e) Ni@NiCu-20 catalysts at different temperatures in a mixed solution of 0.15 M $NaBH_4$ and 2 M NaOH at a scan rate of 10 mV s^{-1}.

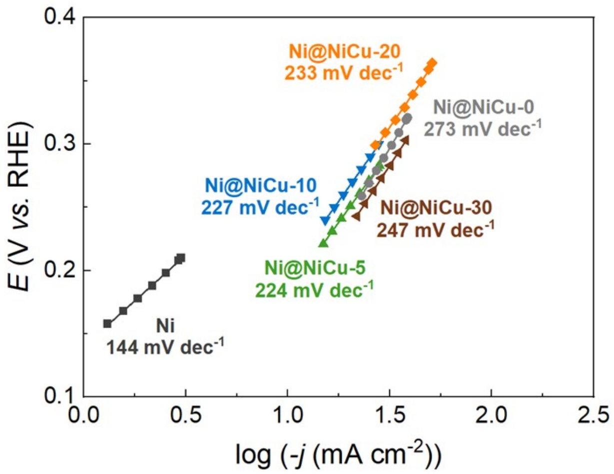

Fig. S12 The Tafel curves of HER on Ni@NiCu-x and Ni catalysts in 2 M NaOH solution at 25 °C.

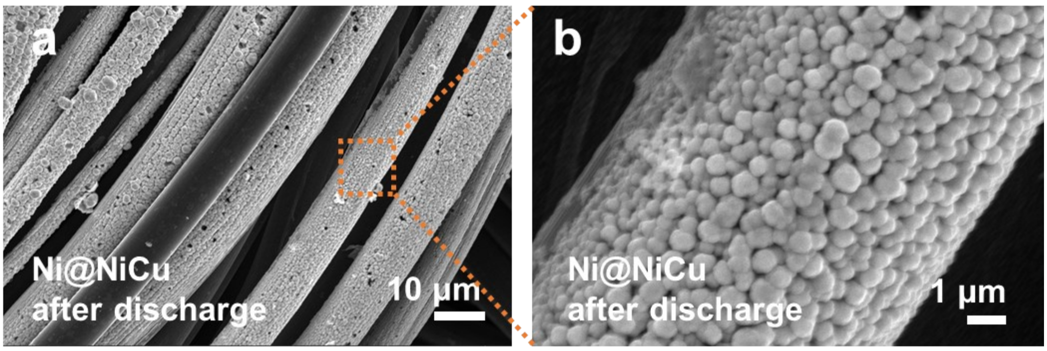

Fig. S13 SEM images of Ni@NiCu-20 after discharge.

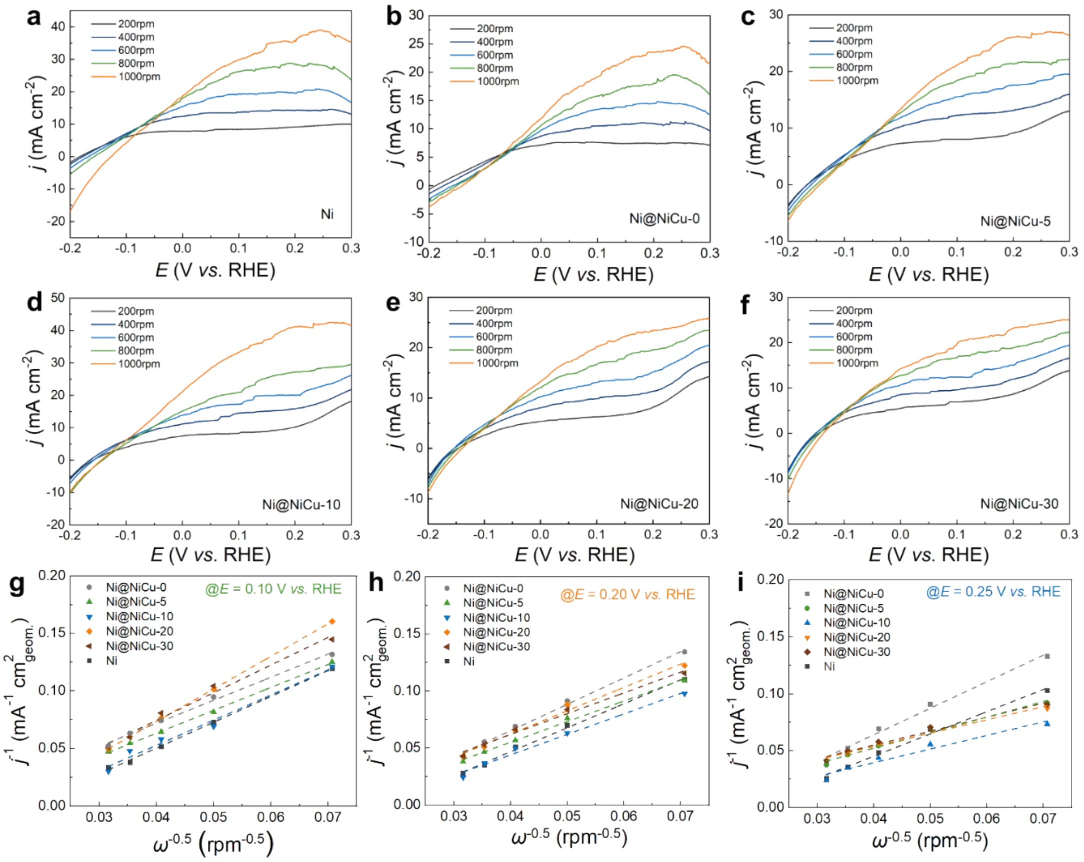

Fig. S14 CV curves of BOR on (a) Ni, (b) Ni@NiCu-0, (c) Ni@NiCu-5, (d) Ni@NiCu-10, (e) Ni@NiCu-20, and (f) Ni@NiCu-30 catalyst electrodes at various rotate speeds; Koutecky-Levich plots of BOR on Ni@NiCu-x and Ni catalyst electrodes at (g) 0.10 V, (h) 0.20 V, and (i) 0.25 V *vs.* RHE.

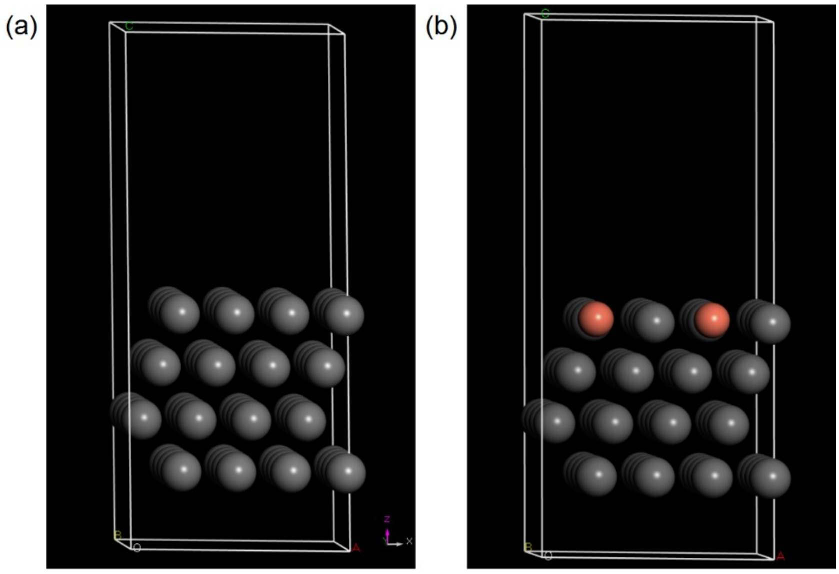

Fig. S15 Surface structure of (a) Ni-0% and (b) Ni@NiCu-2%, the grey and orange denote Ni and Cu atoms, respectively.

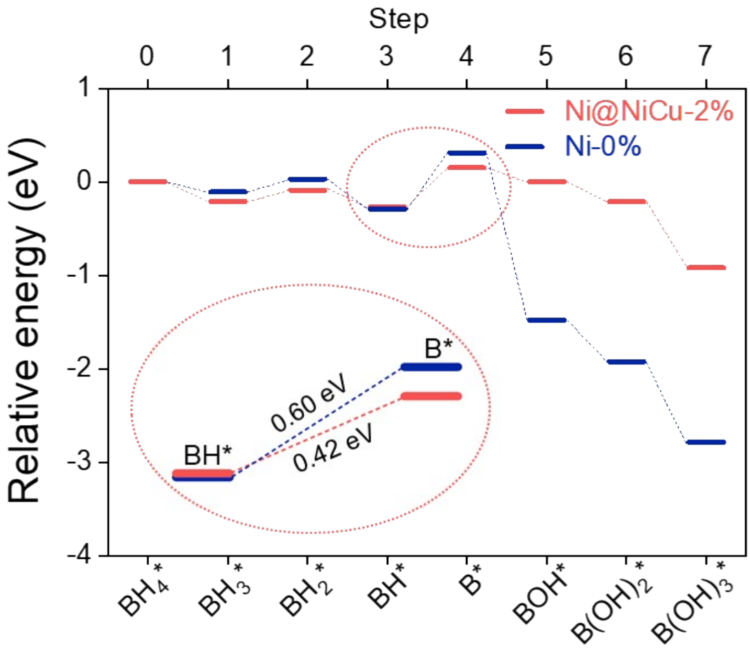

Fig. S16 Reaction pathway of BOR on Ni@NiCu-2% and Ni-0% at 0 V *vs.* RHE.

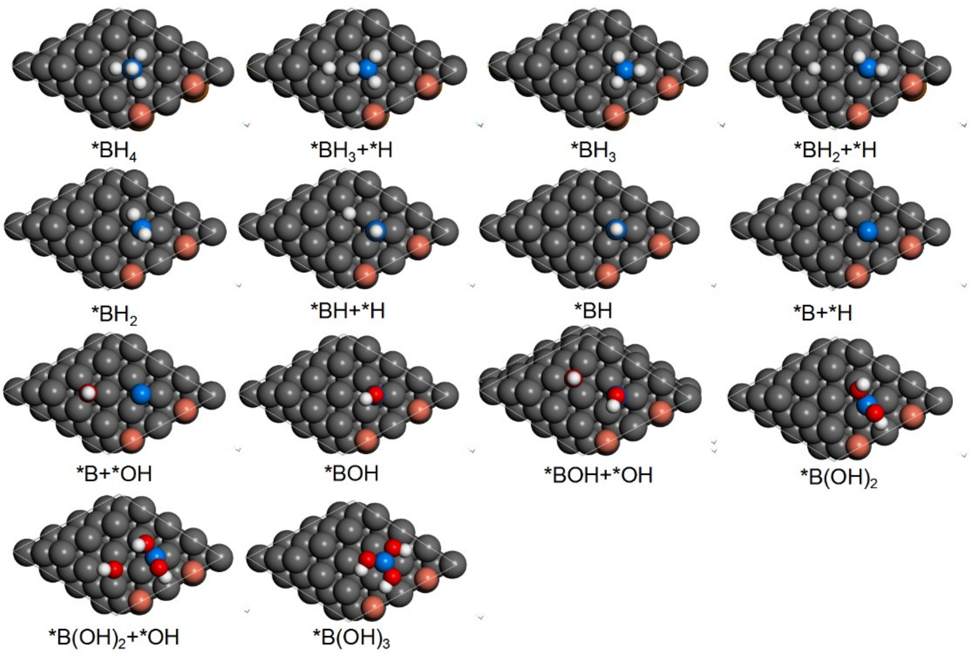

Fig. S17 Optimized structures of corresponding reaction intermediates in BOR on the Ni@NiCu-2% surface, the Ni, B, O and H atoms are denoted by gray, blue, red, and white balls, respectively.

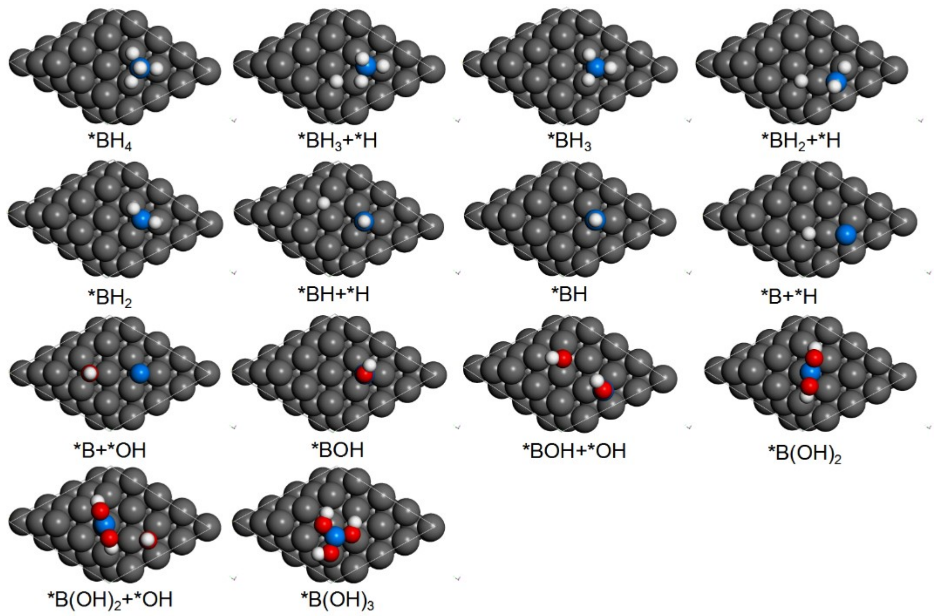

Fig. S18 Optimized structures of corresponding reaction intermediates in BOR on the Ni-0% surface, the Ni, B, O and H atoms are denoted by gray, blue, red, and white balls, respectively.

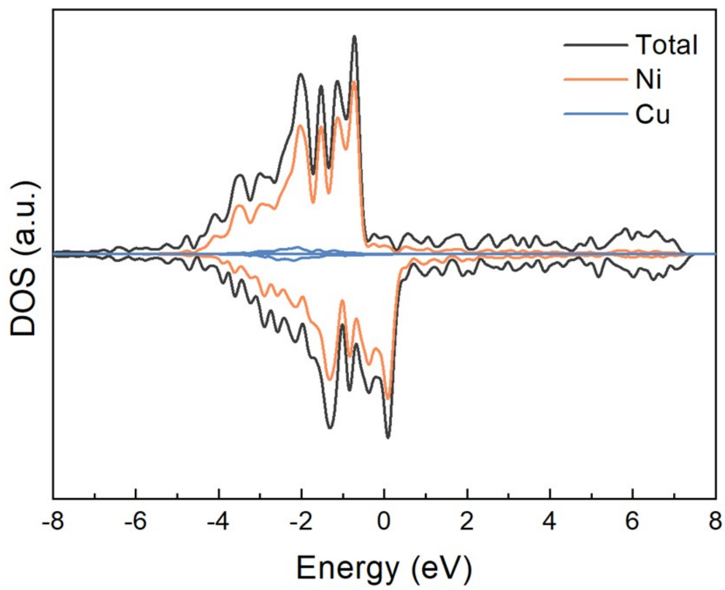

Fig. S19 Projected DOS of the Ni@NiCu-2%.

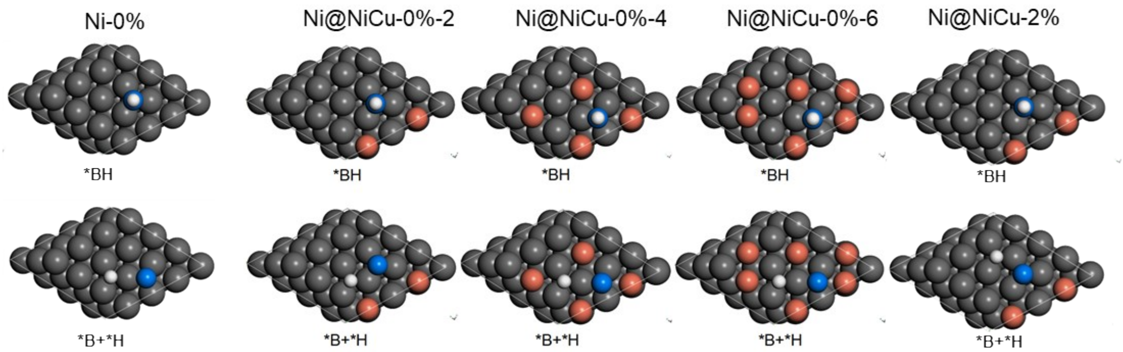

Fig. S20 Optimized structures of corresponding reaction intermediates in BOR on the Ni-0%, Ni@NiCu-0%-x, and Ni@NiCu-2% surface, the Ni, B, O and H atoms are denoted by gray, blue, red, and white balls, respectively.

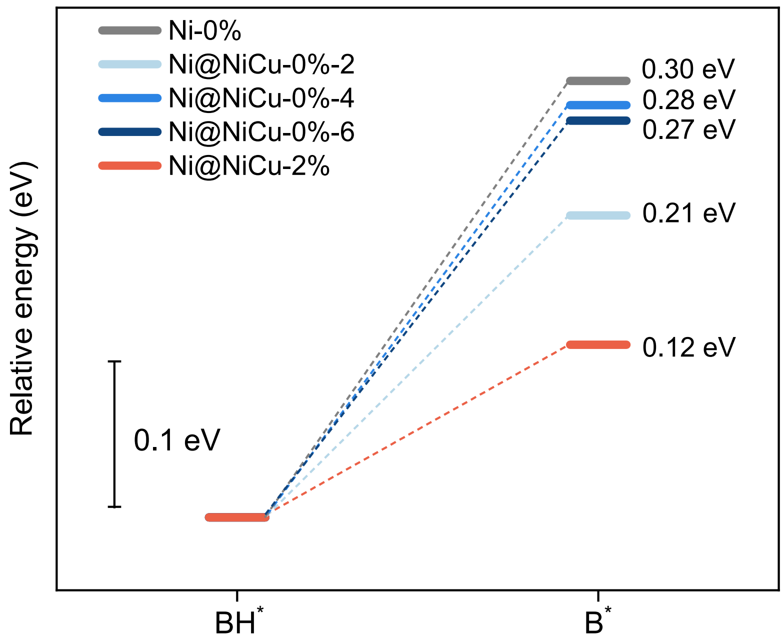

Fig. S21 Energy barrier for the fourth decoupling of B-H bond on Ni-0%, Ni@NiCu-0%-x, and Ni@NiCu-2% at 0.3 V *vs.* RHE.

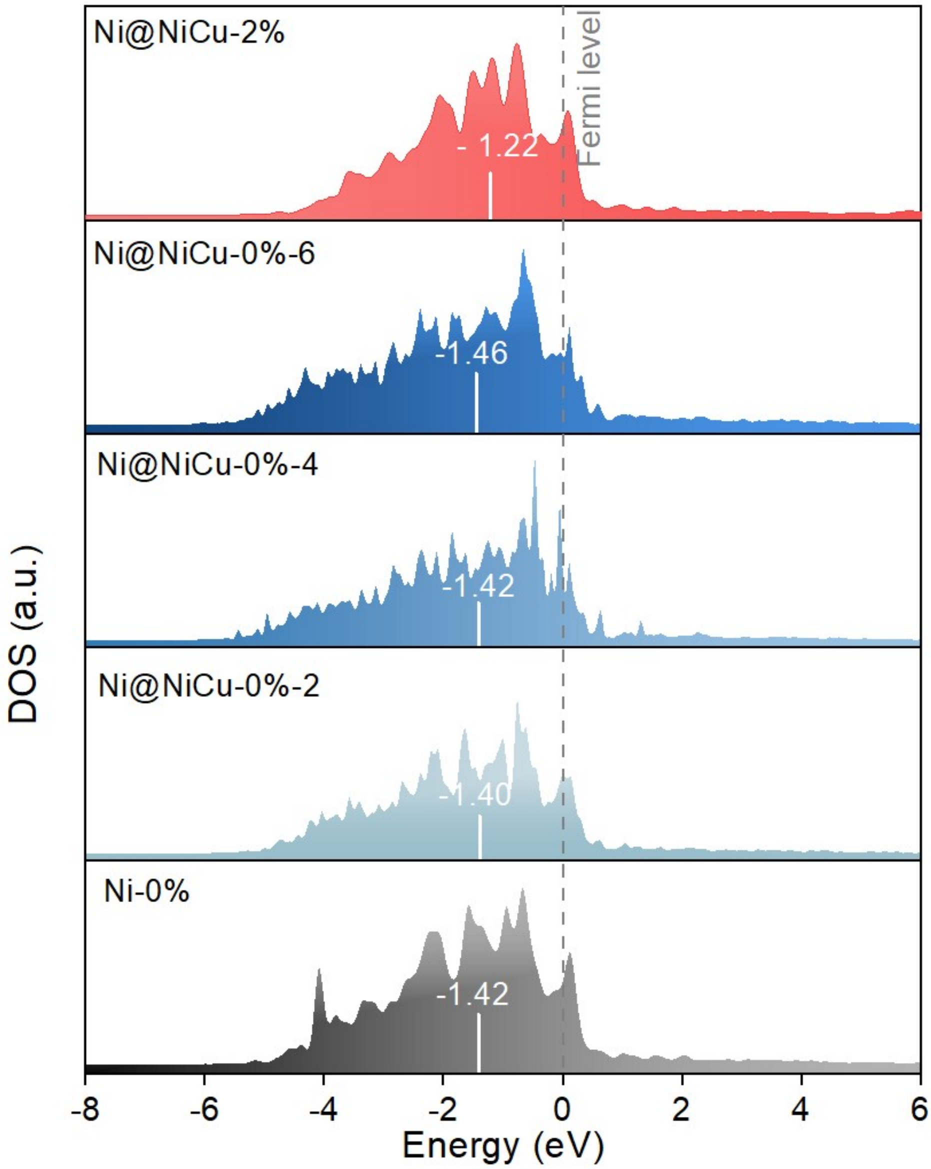

Fig. S22 Comparison of the density of state of 3d orbitals of Ni-0%, Ni@NiCu-0%-x, and Ni@NiCu-2%.

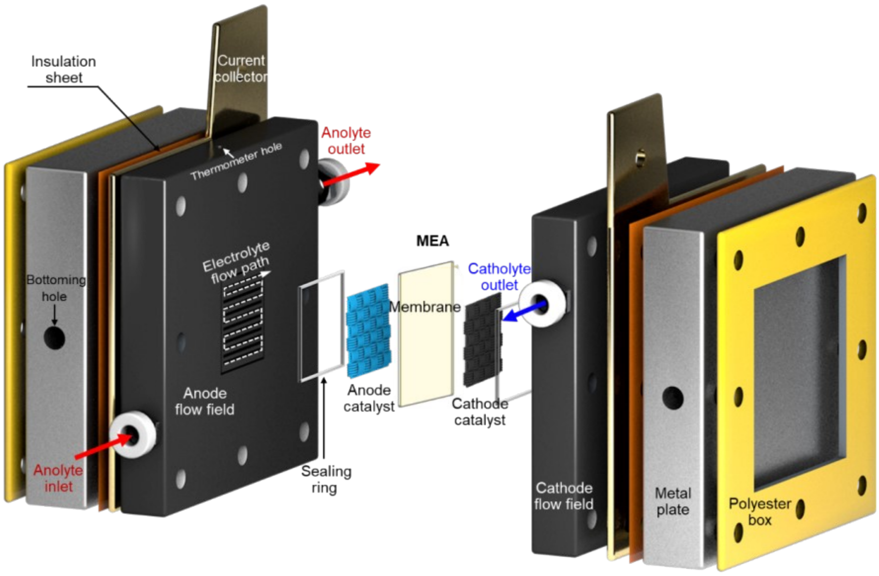

Fig. S23 Configuration schematic diagram of DBFC unit.

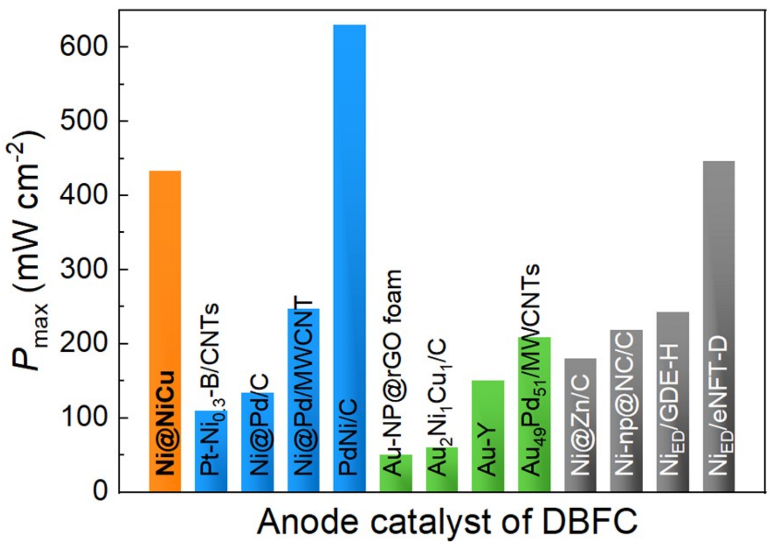

Fig. S24 Performance comparison of DBFCs.

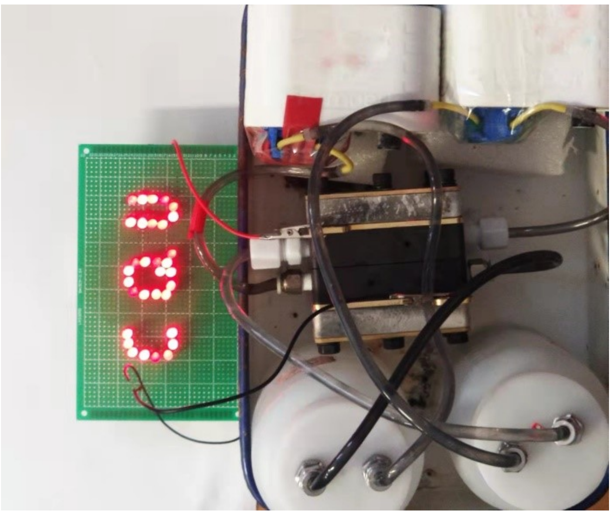

Fig. S25 Practical application of the DBFC with the Ni@NiCu anode.

Table S1 XRD refinement results of prepared catalysts.

Catalyst	lattice parameter (Å)	ε_{micro} (%)	SA-ε_{micro} (%)
Ni	3.522253	0.058321	0.00269
Ni@NiCu-0	3.523355	0.011008	0.0004
Ni@NiCu-10	3.524195	0.203011	0.016424
Ni@NiCu-20	3.524439	0.062177	0.005174
Ni@NiCu-30	3.5244392	0.021008	0.00062

Table S2 Summaries of electrocatalytic activities of prepared catalysts towards BOR.

Catalyst	j @0.3 V (mA cm^{-2})	Tafel slope (mV dec^{-1})	R_{ct} (Ω)	C_{dl} (*mF*)
Ni	132	317	6.10	7.22
Pt/C	69	325	5.48	-
Ni@NiCu-0	135	275	3.51	9.52
Ni@NiCu-5	177	267	2.61	8.89
Ni@NiCu-10	219	240	1.68	7.98
Ni@NiCu-20	246	163	1.08	8.41
Ni@NiCu-30	198	211	2.15	7.27

Table S3 The catalytic activities to BOR (at ~ 0.3 V *vs.* RHE) achieved by some typical noble-metal-based and Ni-based catalysts developed in recent years.

Catalyst	Testing condition	j_{ECSA} (mA $cm^{-2}_{Cat.}$)	Reference
Ni@NiCu-20	**0.15 M $NaBH_4$ + 2 M NaOH**	**6.57**	**This work**
PdNi/C	0.05 M $NaBH_4$ + 1 M KOH	0.45	[3]
Pd/C	0.05 M $NaBH_4$ + 1 M KOH	0.15	[3]
Co-Ni-B	0.1 M KBH_4 + 1 M KOH	0.55	[4]
Ni_{ED}/eNFT	0.05 M $NaBH_4$ + 1 M NaOH	0.13	[5]
Ni-np@NC	0.135 M $NaBH_4$ + 2 M NaOH	2.14	[6]
Ni@Zn	0.135 M $NaBH_4$ + 2 M NaOH	1.8	[7]
$Pt_{67}Fe_{33}$/C	0.1 M $NaBH_4$ + 3 M NaOH	1.64	[8]
$Cu_{51}Ni_{37}Pd_{12}$@Ni foam	0.3 M $NaBH_4$ + 2 M NaOH	0.15	[9]

Reference

1 A. Roustila, C. Severac, J. Chêne and A. Percheron-Guégan, *Surf Sci*, 1994, **311**, 33–44.

2 Z. Huang, Z. Chen, Z. Chen, C. Lv, H. Meng and C. Zhang, *ACS Nano*, 2014, **8**, 8121–8129.

3 S. Saha, P. Gayen, Z. Wang, R. J. Dixit, K. Sharma, S. Basu and V. K. Ramani, *ACS Catal*, 2021, **11**, 8417–8430.

4 Y. e. Duan, S. Li, Q. Tan, Y. Chen, K. Zou, X. Dai, M. Bayati, B. B. Xu, L. Dala and T. X. Liu, *Int J Hydrogen Energy*, 2021, **46**, 15471–15481.

5 G. Braesch, Z. Wang, S. Sankarasubramanian, A. G. Oshchepkov, A. Bonnefont, E. R. Savinova, V. Ramani and M. Chatenet, *J Mater Chem A Mater*, 2020, **8**, 20543–20552.

6 B. Hu, J. Yu, J. Meng, C. Xu, J. Cai, B. Zhang, Y. Liu, D. Yu, X. Zhou and C. Chen, *ACS Appl Mater Interfaces*, 2022, **14**, 3910–3918.

7 B. Hu, P. Chen, C. Xu, J. Meng, J. Cai, Y. Yang, B. Zhang, D. Yu, X. Zhou and C. Chen, *Appl Catal B*, 2022, **307**, 121183.

8 L. Yi, B. Yu, W. Yi, Y. Zhou, R. Ding and X. Wang, *ACS Sustain Chem Eng*, 2018, **6**, 8142–8149.

9 C. Song, G. Wang, B. Li, C. Miao, K. Ma, K. Zhu, K. Cheng, K. Ye, J. Yan, D. Cao and J. Yin, *Electrochim Acta*, 2019, **299**, 395–404.